Effect of rock mass intactness on tunnel safety and stability in blasting excavation

Pingyuan Yang[1], Xiaoen Wu[2,*], Junhua Chen[3]

1. Institute of Mineral Resources, Chinese Academy of Geological Sciences, Beijing 100037, China

2. China Energy Engineering Group Equipment Co. Ltd., Beijing 100044, China

3. School of Civil Engineering, Central South University, Changsha 410075, China

xewu@ceec.net.cn

ABSTRACT. *This paper attempts to make an accurate assessment of the safety and stability of tunnels in blasting excavation, considering the effect of rock mass intactness. For this purpose, numerical simulations and field tests of tunnel blasting excavations were carried out in rocks with different intactness indexes. For simplicity, the multi-hole blasting load was replaced with the equivalent blasting load according to the Chapman-Jouguet (C-J) detonation mechanism and the theory of stress wave propagation in elastic medium. Then, the existing blasting damage model of rock mass was improved into a continuum damage model of rock blasting considering the intactness of rock mass, and imported to FLAC3D for numerical simulations of tunnel blasting excavation. The simulation results were then verified through field tests on blasting vibration velocity and acoustic wave velocity. The attenuation law of blasting vibration was obtained from the tests on blasting vibration velocity, while the blasting-induced fracture zone was determined through the tests on acoustic wave velocity in the borehole before and after blasting. The blasting-induced fracture zone near the explosion sources and the attenuation law of blasting vibration velocity far from the sources were both identified in the numerical simulations and the field tests. After that, the results of the numerical simulations were compared with those of the field tests. The comparison shows that: after the blasting excavation of pressure diversion tunnels, the maximum and the minimum depths of blasting-induced fracture in the surrounding rock respectively appeared at the haunch and the vault of tunnels; when the drilling and blasting parameters remained constant, the maximum depth of blasting-induced fracture and several other factors decreased significantly with the growth of the intactness index; meanwhile, the vibration-influenced distance of blasting increased first and then decreased. The results of numerical simulations agree well with those of the field tests. The research findings provide valuable guidance to blasting excavation of pressure diversion tunnels.*

RÉSUMÉ. *Dans le contexte de l'excavation par dynamitage de tunnels de dérivation de pression dans la centrale hydroélectrique Xi Luodu en Chine, le but de cette étude, c'est de fournir des références à l'évaluation de la sécurité et de la stabilité du tunnel pendant les excavations, à laquelle l'influence de la masse rocheuse devrait être considérée. Pour atteindre ce but, des simulations numériques et des essais sur le terrain d'excavations par soufflage dans des tunnels*

ont été effectués dans les roches avec des indices d'intégrité différents. Visant à simplifier la simulation numérique du dynamitage à trous multiples, une méthode d'utilisation de charges de dynamitage équivalentes pour remplacer la charge de dynamitage à trous multiples a été présentée, selon le mécanisme de donation C-J et la théorie de la propagation des ondes de contrainte en milieu élastique. Un modèle de dommage continu du dynamitage de roche en raison de l'état intact de la masse rocheuse est établi en améliorant le modèle de dommage de dynamitage existant de roche. Le modèle établi a été importé dans le logiciel FLAC3D pour les simulations numériques de l'excavation par dynamitage des tunnels et les charges de dynamitage dans les simulations sont basées sur la méthode présentée. Des essais sur le terrain de la vitesse de vibration du dynamitage et de la vitesse de l'onde acoustique ont été effectués pour vérifier les résultats de la simulation numérique. Les essais de vitesse des ondes acoustiques ont été effectués dans le trou de forage avant et après le dynamitage pour déterminer la zone de fracture induite par le dynamitage. Les tests de vitesse de vibration de dynamitage ont été utilisés pour obtenir les lois d'atténuation de la vibration de dynamitage. Les simulations numériques et les essais sur le terrain ont permis d'obtenir la zone de destruction près des sources d'explosion et la loi d'atténuation de la vitesse de vibration des explosions éloignées des sources d'explosion. Les résultats obtenus par des simulations numériques et des tests sur le terrain ont été comparés. Les résultats montrent que, pour l'excavation par dynamitage de tunnels de détournement de la pression, la profondeur maximale et minimale de fracture induite par le dynamitage de la roche environnante se situent respectivement à l'intersection et à la voûte des tunnels. Dans les conditions où les paramètres de forage et de dynamitage restent constants, la profondeur maximale de fracture induite par le dynamitage, ainsi que le coefficient d'influence du site et l'atténuation de la formule de Sadaovsk qui permet de prédire la vitesse maximale influencée par les vibrations, diminuent de façon significative avec l'augmentation de la indice d'intégrité. La distance de dynamitage influencée par les vibrations augmente tout d'abord, puis diminue avec l'augmentation de l'indice d'intégrité. Les résultats obtenus des simulations numériques sont en bon accord avec ceux des essais sur le terrain. Les résultats de la recherche servent de guides pour l'excavation par dynamitage des tunnels de dérivation dans la centrale hydroélectrique de Xi Luodu.

KEYWORDS: *hydropower plant; pressure diversion tunnel, numerical simulation, the intactness index, blasting vibration velocity, acoustic wave velocity.*

MOTS-CLÉS: *centrale hydroélectrique, tunnel de dérivation de la pression, simulation numérique de dynamitage, l'indice d'intégrité de la masse rocheuse, vitesse maximale de la vibration de dynamitage, vitesse de l'onde acoustique.*

DOI:10.3166/ACSM.42.75-101 © 2018 Lavoisier

1. Introduction

Assessment of safety and stability on tunnels during rock blasting excavation is important and indispensable, focusing on the blasting-induced fracture zone near the explosion sources and the blasting vibration propagation zone, outside the blasting-induced fracture zone. The blasting dynamic responses in the two zones were studied through field test and numerical simulation of blasting. The most common field tests include the acoustic wave velocity test and the blasting vibration test, as seen from the references (Ramulu *et al.*, 2009; Saiang, 2010; Chen *et al.*, 2015; Zhao *et al.*, 2016). The acoustic wave velocity test, which is conducted before and after blasting, in the

borehole, is used to determine the blasting-induced fracture zone. The blasting vibration test, which includes the vibration velocity test and the accelerated, is conducted during blasting to gain the vibration-influenced distance of blasting. LS-DYNA, ABQUS and FLAC3D are commonly used in the numerical simulations of blasting, as seen from the references (Ma & An, 2008; Wang & Konietzky, 2009; Saiang, 2010; Cai & Zhang, 1997).

Blasting excavations are actually conducted in rock mass rather than in homogeneous rocks, and the mechanical properties of the rock mass are mainly decided by the rocks and the intactness of the rock mass. According to Bhandari and Badal (1990), the discontinuity of rock affected the blasting fracture effects. However, through the summaries of the related research, Chen *et al.* (2016) clear that, the current research of numerical simulation of blasting scarcely considered the influences of the intactness of the rock mass on the safety and stability of the tunnels during the blasting excavation. Li *et al.*, (2010) point out that, currently, the most commonly used constitutive models in the numerical simulations of blasting are the continuum damage constitutive models of blasting, as seen from the references (Kipp & Grady, 1980; Taylor *et al.*, 1985; Taylor *et al.*, 1986; Chen & Taylor, 1986; Kuszmaul, 1987). Through the user-defined import modes or other methods, scholars commonly put the continuum damage constitutive models of blasting into the generic software of numerical simulation, like LS-DYNA, ABQUS and FLAC3D. In fact, not only the rock material but also the rock mass commonly contains defects inside, that is to say, both the rock mass and the rock material are usually the media in certain damage state before loading, according to the damage mechanics. The influence of the original defects on damage developments can't be analyzed through the current continuum damage constitutive model, that is the serious drawback to stop the current numerical simulation of blasting from being used in considering the influences of rock mass intactness.

In order to have the existing and prevalent constitutive models in accordance with the truth, scholars are trying their best to improve the models. For examples, based on the continuum model of explosive fracture presented by Grady and Kipp (1980), Taylor *et al.* (1985) established a continuum damage model of brittle rock under blasting. As the effects induced by high densities of microcracks were not considered by Taylor *et al.* (1986), Kuszmaul (1987) improved the damage model. The damage evolution expression in the continuum damage model presented respectively by Yang *et al.* (1996) and Liu and Katsabanis (1997) are simpler than those presented by Kuszmaul. In the light of the continuum damage mechanics and the theory of stress wave, Zhu and Yu (2001) given the relations among the damage variable, the velocity of acoustic wave and the intactness index of rock mass for the purpose of determining the fracture zone induced by blasting, which provided an idea to improve the existing continuum damage constitutive model.

In addition to the constitutive model, there is another problem in the numerical simulation of tunnel blasting excavation. Blasting of tunnel excavation belongs to multi-holes blasting. Since the numerical simulation of multi-holes blasting will bring difficulties to the numerical modeling and solution, the numerical simulation of the tunnel blasting excavation generally does not completely set up all the blast hole units

according to the actual situation, but uses the simplified equivalent loading. For example, in the numerical simulation of tunnel blasting excavation, Zuo *et al.* (2011) put the equivalent load caused by the perimeter hole blasting on the contour of tunnels, considering only the blasting damage caused by the perimeter hole, ignoring the blasting vibration caused by the breaking hole blasting. That is not very sustainable to the safety- stability assessment of tunnel during blasting excavation, because the blasting vibration is mainly caused by the breaking hole blasting and the blasting vibration assessment plays an important role in the safety- stability assessment. Therefore, the simplified numerical simulation must simultaneously take into account the of the dynamic response solution in the fracture zone and the vibration zone.

The underground cavern group excavation of Xi Luodu Hydropower Station in China belongs to a large-scale excavation project of deep-buried caverns. The pressure diversion tunnels play an important part in the structures of the hydropower station. The initial damage degree or intactness of rocks is highly discrete for the pressure diversion tunnels, so that the influences from the intactness of rocks on blasting effects must be considered. In order to provide guides to the blasting excavation projects like the pressure diversion tunnels having to consider the influences of the rock mass intactness, this study attempts to establish a blasting-induced damage model of rock on account of the initial damage or the intactness, and use equivalent blasting loading method to carry out the numerical simulation of blasting excavation of the pressure diversion tunnels. Meanwhile, field test corresponding to the numerical simulations are also carried out to check the results of the numerical simulation. The blasting-induced fracture zone and the propagation of blasting vibration velocity were gained by the study, for the purpose of safety-stability analysis of the pressure diversion tunnels.

2. The blasting excavation of tunnels

Xi Luodu Hydropower Station is currently the third largest of its kind in the world and one of several large-scale cascade hydropower stations developed in the Jinsha River Basin, in China. There are 9 parallel pressure diversion tunnels on the left and right banks of the hydropower station. Their excavation procedure is divided into the following five sections along the elevation reduction direction: upper flat section, upper curved section, vertical shaft section, lower curved section and lower horizontal section. The lower horizontal section has a length of about 60m, a vertical burial depth of 400-500m, and a horizontal depth of about 300m. For the original rock near the lower horizontal section, the vertical stress is about 9 MPa, the horizontal stress along the axis of the hole is about 6 MPa, and the horizontal stress in the direction of the vertical axis is about 16 MPa. The excavated bedrock is hard basalt with uniaxial compressive and tensile strengths of 100 MPa and 10 MPa, respectively. The total length of the pressure diversion tunnel in the lower horizontal section is about 540 meters, and the average wave velocity of the rock acoustic wave is about 4300 m/s. The sound velocity distribution ranges from 3600 to 5600 m/s. The intactness of surrounding rocks of the same pressure diversion tunnel show little difference, but those of different pressure diversion tunnels have greater discreteness. The intactness

of the surrounding rock of the pressure diversion tunnel group is described as intact - relatively broken. Its intactness index ranges from 0.20 to 0.80. Groundwater is not very abundant. The surrounding rocks mainly belong to categories II and III, but few to I. The pressure diversion tunnel in the lower horizontal section has a circular cross-section, and it is excavated respectively from upper and lower layers. The excavation area of the upper layer is larger, accounting for about 80% of the total excavation area. The research object of this study is excavation blasting of the upper layer of pressure diversion tunnel in the lower horizontal section. The radius of tunnel excavation cross-section is 5.9 m. The cross-section of the drilling hole distribution for the blasting excavation of the upper layer of pressure tunnel is shown in Figure 1. In Figure 1, Ms3 to Ms15 indicate the detonator section umber. As the number increases from 3 to 15, the detonator delay blasting time increases. Among them, Ms3 corresponds to the blasting of the cut hole, Ms12 that of the cushion hole, Ms13 that of the perimeter hole (hole of smooth blasting), and the remaining detonator sections correspond to the breaking holes (the major blast holes). The main blasting parameters are shown in Table 1. When considering the influence of the intactness of the rock, the on-site blasting construction adjusts the blasting parameters based on Figure 1 and Table 1.

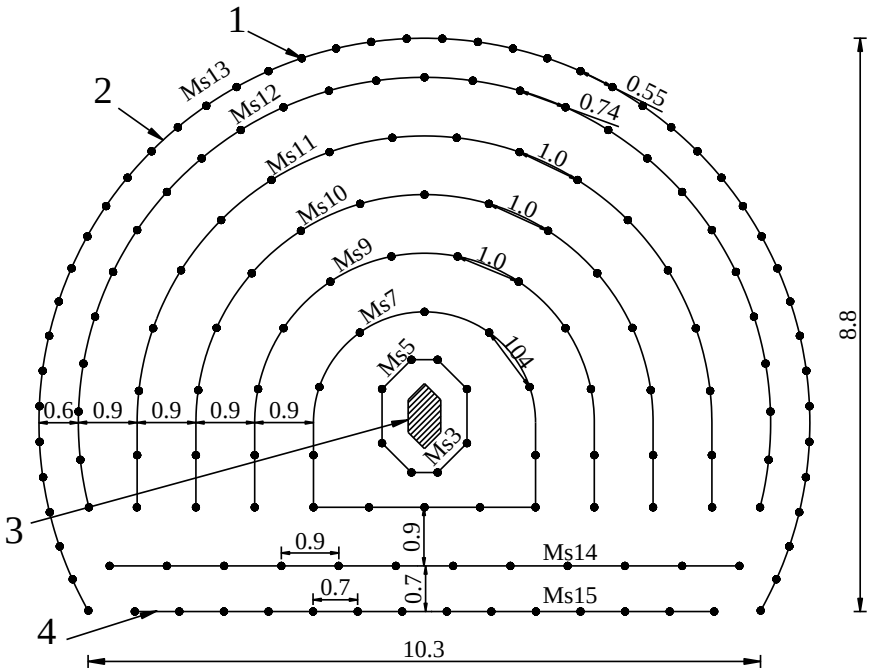

1-blast hole, 2-tunnel contour, 3- cutting blasting zone, 4- floor of the upper

Figure 1. Section of drilling layout for upper blasting excavation of pressure diversion tunnel (unit: m)

Table 1. Parameters of blasting excavation of upper layer of pressure diversion tunnel

Borehole Names	Borehole diameter/mm	Borehole Length /m	Borehole Number	Cartridge diameter /mm	Cartridge Length /m	Single-hole explosive charge /kg	Maximum explosive charge of single-section detonation /kg
Cut hole	50	3.3	7	35	2.4	2.6	18.2
Breaking hole	50	3.0	91	35	2.2	2.4	43.2
Cushion hole	50	3.0	27	35	1.2	1.4	37.8
Perimeter hole	50	3.0	46	25	1.0	0.6	27.6

3. Simulation of multi-holes blasting for tunnel excavation

3.1. Single-hole blasting

The blast hole is short due to the short tunnel excavation footage. According to the C-J detonation model, it is assumed that the instantaneous detonation of the explosive in the blast hole generate detonation products, which expand and act on the hole wall to produce the cylindrical waves. The 2 # rock emulsion explosive is commonly used in excavation blasting of hydraulic tunnels. When the emulsion explosive explodes, the peak blasting pressure per unit area on the wall of a single hole is:

$$p_{\max} = \begin{cases} \dfrac{n\rho_e c_j^{\,2}(\gamma_a\gamma_r^2)^{-\kappa_1}}{(2\kappa_1+2)} & p_{\max} \geq np_k \\ np_k\left(\gamma_a\gamma_r^2\right)^{-\kappa_2}\left[\dfrac{\rho_e c_j^{\,2}}{p_k(2\kappa_1+2)}\right]^{\kappa_2/\kappa_1} & p_{\max} \leq np_k \end{cases} \quad (1)$$

where, ρ_e is the cartridge density of 2 # rock emulsion explosive, with a the value of 1200 kg / m^3; c_j the detonation velocity of the emulsion explosive cartridge, with a value of 3800 m/s; κ_1 and κ_2 high pressure and low pressure expansion indexes, respectively, and κ_1=2-3 and κ_2=1.2-1.4; p_{max} the peak pressure per unit area on the inner boundary surface of the blast hole; p_k the critical expansion pressure per unit area, and p_k=200*MPa*; and γ_a and γ_r the uncoupling coefficients of axial and radial charges, respectively. According to Table 1, for perimeter holes, γ_a =1.83 and γ_r =2.00. For the perimeter hole and the breaking hole, γ_a =1.00 and γ_r =1.43; and n is the dynamic pressure enhancement coefficient, and n=8-11.

The explosion pressure at any time on the hole wall is calculated in the form of an exponential function, and its expression is (Li, 1994):

$$p(t) = p_{\max} \cdot \chi_3 \cdot (e^{-\chi_1 t} - e^{-\chi_2 t}) \tag{2}$$

Where, $p(t)$ is the explosion pressure acting on the unit area of the hole wall at time t; χ_1-χ_3 are the calculation parameters.

3.2. Equivalent load of the multi-holes blasting

As shown in Figure 1 above, there are many blast hole units for pressure tunnel excavation blasting, thus the modeling according to actual conditions often poses challenges to calculation and analysis. Therefore, the blasting excavation model is simplified based on the following points:

a. The center of the excavation section is regarded as the blasting center, and the area where the explosion stress wave propagates from the blasting center to the outside is the region under the influences of blasting damage and blasting earthquake. The near zone of the explosion defines the range under the impact of the blasting damage, wherein the rock is damaged, with deteriorating mechanical property. The moderately far or far-zones are the blasting seismic wave propagation areas.

b. The cut hole is mainly responsible for breaking the rocks to provide a free surface for the subsequent breaking hole detonation. In contrast to the perimeter hole, the breaking hole has a higher explosive charge but it is far from the digging contour line, while the cushion hole is close to the digging contour line but has a lower explosive charge. Therefore, the damage to the retaining surrounding rock near the excavation contour is mainly caused by the simultaneous blasting of the perimeter holes.

c. According to law of seismic wave attenuation proposed by Sadowski, the maximum vibration intensity in the moderately far or far-zones of explosion corresponds to the maximum explosive charge of single-section detonation. Referring to Figure 1 and Table 1, it can be seen that the maximum explosive charge of single-section detonation corresponds to the breaking hole in the detonator section Ms11.

The safety and stability analysis of surrounding rock in tunnel excavation mainly targets the damage of surrounding rock near the explosion sources and the vibration instability in the moderately far or far-zones. Therefore, the solution of dynamic response of the tunnel under multi-holes blasting can be simplified as that of the dynamic response under the blasting actions of the perimeter holes and the breaking hole with the maximum single-section denotation explosive charge. At present, the equivalent loading boundary is generally set for the simplification of multi-holes blasting model, and the energy or intensity of stress wave applied on the equivalent loading boundary is equal to the original dynamic loading. For perimeter hole blasting, the damage and failure zone near the explosion sources depends mainly on the shape of stress wave or the direction of stress action as well as the intensity of stress wave. According to the formula (1), the blasting damage zone propagates the approximately

cylindrical wave. The shape of the blast hole determines the stress wave loading waveform. Therefore, the shape of the action boundary of the perimeter hole blasting load cannot be changed. The explosion stress in the moderately far or far-zones of the explosion is generally converted from a cylindrical wave to a spherical wave rapidly. Therefore, the loading boundary has little effect on the blasting vibration.

For the breaking hole blasting, the equivalent loading boundary of is composed of the excavation contour line of the retaining surrounding rock and the excavation bottom plate. For the perimeter hole blasting, the equivalent loading boundary is the semi-hole wall of the original perimeter hole on the excavation contour line of the retaining surrounding rock, so that the wavefront of the outward stress wave excited by the perimeter hole blasting from the blasting center is kept as a cylinder. The loading length of the equivalent load along the excavation direction or the axial direction of the cavity is the footage of a single blasting excavation. The boundary of the equivalent blasting load is shown in Figure 2, wherein A and C are the intersection points of the excavation arc and the bottom plate, respectively, and B is the vault. The arc ABC is the excavation contour line, and the line segment AC is the excavation bottom plate.

(1) Equivalent load of the breaking-hole blasting

According to the Huygens wave theory, the medium point on the wavefront can be regarded as the wavelet sources of the external radiation disturbance. Here, the breaking holes that simultaneously detonate in a single section is regarded as the same wavelet sources. According to the theory of stress wave propagation in elastic medium, it is assumed that the energy of stress wave on the loading surface of equivalent blasting load is equal to the total energy of stress wave radiated from the blasting center of each blast hole, e.g., the following formula is satisfied:

$$m \cdot w \cdot S = \overline{w} \cdot \overline{S} \tag{3}$$

Where, w and $\overline{w}$ are the energy density radiated by a single blast hole blasting and the energy density on the loading surface of equivalent blasting load, respectively; m the number of blast holes detonated in the same section; S half of the cylindrical area of the breaking hole per unit length and $\bar{S}$ the equivalent blasting loading surface area per unit length, corresponding to arc ABC and line segment AC in Figure 2.

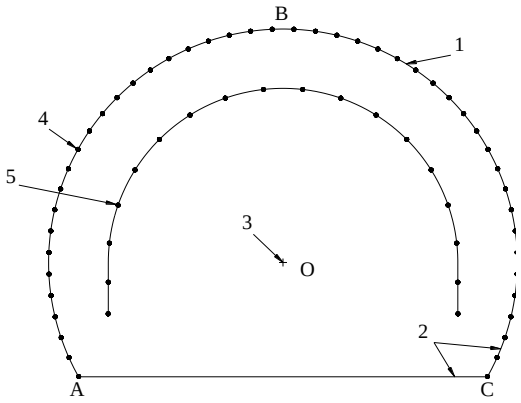

1- Tunnel contour, 2- Equivalent blasting load line of the breaking hole (segment AC and arc ABC), 3- Explosive center, 4- Perimeter holes, 5- Breaking holes

Figure 2. Schematic plot of equivalent blasting loading boundary

When the influence of damping factor is not considered, the explosion stress wave is elastic. When the total energy of the stress wave is constant, the elastic wave energy density is proportional to the square of the stress amplitude. The following relationship is obtained from Formula (3):

$$m \cdot [p_{\mathrm{b}}(t)]^2 \cdot S = [\bar{p}_{\mathrm{b}}(t)]^2 \cdot \bar{S} \tag{4}$$

Where, $\bar{p}_b(t)$ is the equivalent blasting load for the breaking hole blasting on the equivalent loading boundary; $p_b(t)$ is the explosion pressure on the wall of the breaking hole, calculated according to Formula (2).

Combining Formula (2), for the breaking hole blasting, the equivalent blasting load is obtained as follows:

$$\bar{p}_{\mathrm{b}}(t) = p_{\mathrm{b\,max}} \cdot \chi_7 \cdot (e^{-\chi_5 t} - e^{-\chi_6 t}) \cdot (mS / \bar{S})^{0.5} \quad t \geq 0 \tag{5}$$

Where, P_{bmax} is the peak blast pressure on the wall of the breaking hole, calculated by formula (1). The χ_6-χ_7 are the calculation parameters of the blast pressure on breaking holes.

As can be seen from Formula (5), the attenuation factor of the elastic amplitude excited by the equivalent blasting load is 0.5. The amplitude attenuation is mainly caused by the geometric wavefront diffusion, without considering the influence of the damping factor. When the viscous damping factor is taken into account, i.e. the stress wave is an elastic viscous wave, the attenuation factor will increase. According to the relation derived from the Reference (Lu & Hustrulid, 2002), the Formula (5) is rewritten as:

$$\bar{p}_{\mathrm{b}}(t) = p_{\mathrm{b\,max}} \cdot \chi_7 \cdot (e^{-\chi_5 t} - e^{-\chi_6 t}) \cdot (mS / \bar{S})^{\xi} \quad t \geq 0 \tag{6}$$

Where, ξ is the attenuation factor taking into account the damping effect, and $0.5 \leq \xi \leq 2$. When $\xi = 0.5$, the blast stress wave is an elastic wave.

(2) The equivalent load of the perimeter-hole blasting

The equivalent blasting load on the wall of the perimeter hole is the same as that of the original blast hole. According to formula (2), with consideration of the blasting delay, the equivalent blasting load on the wall of the perimeter hole is calculated as:

$$\bar{p}_{\mathrm{p}}(t) = p_{\mathrm{pmax}} \cdot \chi_{10} \cdot [e^{-\chi_8 (t-\tau)} - e^{-\chi_9 (t-\tau)}] \quad t \geq \tau \tag{7}$$

Where, $\bar{p}_b(t)$ is equivalent load of perimeter hole blasting; t the interval between the blasting of breaking hole and that of the perimeter hole; P_{pmax} the peak blast pressure on the perimeter hole, and χ_8-χ_{10} the calculation parameters of blast pressure.

4. Constitutive model of blasting damage considering the intactness of rock mass

4.1. Damage evolution law considering the influence of initial damage

Rock is prone to brittle failure under tensile condition, and plastic failure under the condition of high pressure. Take rock damage variables as scalar. In the tensile state, according to the continuum damage model of blasting presented by Chen *et al.*, the damage variable can be expressed as a probability function with the crack density as a variable, and its expression is:

$$D = D_{\mathrm{t}} = 1 - \exp(-a_1 N^{a_2}) \tag{8}$$

Where, D is the per unit damage variable of rock, D_{t} the tensile damage variable; and N the crack density, indicating the number of cracks per unit length. a_1 and a_2 are calculation parameters for material damage.

The crack density N is calculated as follows:

$$N = \int_0^t a_3 (-\theta + \theta_{\mathrm{lim}})^{a_4} \, \mathrm{d}t + N_0 \tag{9}$$

Where, θ is equivalent tensile strain, and $\theta < \theta_{\mathrm{lim}}$. The negative sign "-" before θ indicates that tension is negative and compression positive. $\theta_{\mathrm{lim}} < 0$, which is the critical value of equivalent tensile strain, related to the initial crack density. a_3 and a_4 are material parameters, N_0 the initial crack density, meaning that the cracks of rock exist before blasting. t is the time.

The initial damage degree is calculated as:

$$D_0 = 1 - \exp(-a_1 N_0^{a_2}) \tag{10}$$

The equivalent tensile strain is calculated as [21]:

$$\theta = -\sqrt{\sum_{i=1}^{3} [\langle -\ln(1+\varepsilon_i)\rangle \cdot \langle -\ln(1+\varepsilon_i)\rangle]} \tag{11}$$

Where, D_0 is the initial damage degree; ε_i is the principal strain in direction I; the engineering strain. $\ln(1+\varepsilon_i)$ is the logarithmic principal strain in the direction i; the operation relationship of the symbol "⟨⟩" is $\langle x\rangle=(x+|x|)/2$, and x is a variable;

The equivalent tensile strain critical value is calculated as:

$$\theta_{\lim} = a_5 N_0^{a_6} \tag{12}$$

Where, a_5 and a_6 are material parameters.

The crack density growth rate is calculated as:

$$\dot{N} = a_3(\theta - \theta_{\lim})^{a_4} \tag{13}$$

The rock damage evolution law is obtained from Formulas (8), (9) and (13):

$$\dot{D} = \dot{D}_t = e^{-[\int_0^t a_1 a_3 (\theta-\theta_{\lim})^{a_4} dt + a_1 N_0)]^{a_2}} \cdot a_1 a_2 (\theta_i - \theta_{\lim})^{a_2 - 1} \tag{14}$$

Where, $\dot{D}_t$ is evolution rate for tensile damage.

Combining Formulas (8), (9) and (11), it can be seen that tensile damage occurs in the rock unit when $\theta<\theta_{\lim}<0$. When $\theta>\theta_{\lim}$, if the rock unit is destroyed, its failure mode will be the plastic damage [15], then the failure criterion satisfies the following formula:

$$F = \sqrt{\frac{1}{2} s_{ij} s_{ij}} - 3\lambda_1 \sigma_m - \lambda_2 (1 - D_c) = 0 \tag{15}$$

Where, F is the expression of Drucker-Prager failure criterion; σ_m the nominal hydrostatic pressure component; s_{ij} the component of the nominal stress partial tensor and Dc the plastic compression damage variable. λ_1 and λ_2 are material parameters.

The relationship between the plastic compression damage variable D_c and the tensile damage variable D_t satisfies the following Formula (Furlong *et al.*, 1990):

$$\dot{D}_c = \lambda_3 \dot{W}_p (1 - D_t) \tag{16}$$

$$W_{\mathrm{p}} = \int \sigma_{ij} \mathrm{d}\varepsilon_{ij}^{\mathrm{p}} \tag{17}$$

In Formulas (16)-(17), W_p is plastic work; ε_{ij}^{p} is the component of plastic strain tensor; σ_{ij} the component of the nominal stress tensor and λ_3 the sensitivity coefficient for tensile damage.

4.2. Constitutive relationship

The relationship between the initial bulk modulus, the initial shear modulus and the volume and shear modulus of the non-damaged material is as follows:

$$K_0 = (1 - D_0)\hat{K} \tag{18}$$

$$G_0 = (1 - D_0)\hat{G} \tag{19}$$

In Formulas (18) and (19), K_0 and G_0 are the initial bulk modulus and initial shear modulus of the damaged rock; $\hat{K}$ and $\hat{G}$ the bulk modulus and initial shear modulus of the non-damaged rock. Take intact rock as non-damaged rock

The total deformation of the rock unit is divided into elastic deformation and plastic deformation. According to the Lemaitre strain equivalence hypothesis, the elastoplastic damage deformation of the rock satisfies the following relationships:

$$\varepsilon_{\mathrm{m}} = \varepsilon_{\mathrm{m}}^{\mathrm{e}} + \varepsilon_{\mathrm{m}}^{\mathrm{p}} \tag{20}$$

$$e_{ij} = e_{ij}^{\mathrm{e}} + e_{ij}^{\mathrm{p}} \tag{21}$$

$$\varepsilon_{\mathrm{m}}^{\mathrm{e}} = \sigma_{\mathrm{m}}' / (3\hat{K}) \tag{22}$$

$$e_{ij}^{\mathrm{e}} = s_{ij}' / (2\hat{G}) \tag{23}$$

$$\mathrm{d}\varepsilon_{\mathrm{m}}^{\mathrm{p}} = \lambda_4 \frac{\partial F}{\partial \sigma_{\mathrm{m}}} \tag{24}$$

$$\mathrm{d}e_{ij}^{\mathrm{p}} = \lambda_4 \frac{\partial F}{\partial s_{ij}'} \tag{25}$$

$$\sigma_{\mathrm{m}}' = \sigma_{\mathrm{m}} / (1 - D) \tag{26}$$

$$s'_{ij} = s_{ij} / (1 - D) \tag{27}$$

In the Formulas (20)-(27), ε_m is average strain, and ε_m^e and ε_m^p are the corresponding elastic strains and plastic strains; e_{ij} partial strain, e_{ij}^e and e_{ij}^p the corresponding elastic strain and plastic strain. σ'_m and s'_{ij} are effective average hydrostatic pressure and effective deviatoric stress respectively. λ_4 is a plasticity factor.

Combining Formulas (18)-(27), the constitutive relationship of rock rate-related damage considering initial damage is as follows:

$$\dot{\varepsilon}_{\mathrm{m}} = \frac{\dot{\sigma}_{\mathrm{m}}(1-D) + \dot{D}\sigma_{\mathrm{m}}}{3K_0(1-D)^2/(1-D_0)} + \dot{\lambda}_4 \frac{\partial F}{\partial \sigma_{\mathrm{m}}} \tag{28}$$

$$\dot{e}_{ij} = \frac{\dot{s}_{ij}(1-D) + \dot{D}s_{ij}}{2G_0(1-D)^2/(1-D_0)} + \dot{\lambda}_4 \frac{\partial F}{\partial s_{ij}} \tag{29}$$

The relation between the intactness index of rock mass before blasting and the damage variable was given in the established model, so that the changes of the intactness index can be used to consider the influences of rock mass intactness on blasting effects.

4.3. Relations between the initial damage variable and the intactness index of rock & safety criteria for surrounding rock excavation blasting

(1) Relations between the initial damage variable and the intactness index of rock

Underground tunnel excavation generally uses borehole acoustic wave method to evaluate the intactness of surrounding rock. The relationship between rock damage variables and acoustic wave velocity is:

$$D = 1 - (c / \hat{c})^2 \tag{30}$$

Where, c and $\hat{c}$ are acoustic wave velocity of damaged rock and that of non-damaged rock, respectively; $\hat{c}$ generally takes the wave velocity value of the complete bedrock. For pressure tunnels, $\hat{c}$=5600m/s.

The relationship among the initial damage degree, the initial intactness index of the rock mass and the acoustic wave velocity is:

$$D_0 = 1 - \eta = 1 - (c_0 / \hat{c})^2 \tag{31}$$

Where, η and c_0 are respectively the initial intactness index and the acoustic wave velocity of the rock mass. They are the parameters of rock mass before blasting.

(2) Safety criteria related to the initial damage variable or the initial intactness index

According to *Construction Technical Specifications on Rock-Foundation Excavating Engineering of Hydraulic Structures* (DL / T5389-2007) published by *National Development and Reform Commission, the People's Republic of China*, When the acoustic wave velocity at a point in the hole drops to 15% of the original rock wave velocity, it can be determined that there appears macroscopic fracture at the point. According to Formulas (30) and (31), the blast damage threshold corresponding to the edge of the affected range of blasting damage is:

$$D_{\lim} = 0.72D_0 + 0.28 = 1 - 0.72\eta \tag{32}$$

Where, D_{lim} is the threshold of the blasting damage. When $D=D_{lim}$ at a certain point, it can be judged that this part is the edge of the blasting-induced fracture zone. The location of $D \geq D_{lim}$ represents the blasting-induced fracture zone.

(3) Safety analysis on the blasting-induced fracture zone, near the explosion sources

The radial distance from the edge of the fracture zone to the explosive center point of the cross section of tunnel is defined as the blasting-induced fracture radius. The blasting center is shown in Fig.2. According to the geometrical similarity and dimensional analysis of explosion, the relationship between the maximum fracture radius and the acoustic wave velocity of the rock mass and the explosive charge for the single-section detonation of the perimeter hole is as follows:

$$R_{\lim} = \max(R) = b_1 (c_0 / \hat{c})^{b_2} (Q_s / l_b \rho_e)^{b_3} \tag{33}$$

Where, R is the blasting-induced fracture radius; R_{lim} is the maximum blasting-induced fracture radius; and Q_s is the explosive charge for the single-section detonation of the perimeter hole. The numbers b_1-b_3 are the test fitting parameters. The "max" means that the maximum value is taken.

The relationship between the maximum blasting-induced fracture radius of the surrounding rock and the initial damage degree and intactness index that are obtained by Formula (31) are calculated as follows:

$$R_{\lim} = b_4 (1 - D_0)^{b_5} (Q_s / l_b \rho_e)^{b_3} \tag{34}$$

$$R_{\lim} = b_4 \eta^{b_5} (Q_s / l_b \rho_e)^{b_3} \tag{35}$$

In the Formulas (34)-(35), b_4-b_5 are the test fitting parameters.

The blasting-induced fracture depth of the retaining surrounding rock along the radial direction of the tunnel and its maximum value are calculated as follows respectively:

$$\Delta R = R - R_0 \tag{36}$$

$$\Delta R_{\lim} = R_{\lim} - R_0 \tag{37}$$

In the Formulas (36)-(37), ΔR represents the blasting-induced fracture depth of the retaining surrounding rock along the radial direction of the tunnel, $\Delta R_{\lim}$ the maximum value and R_0 tunnel excavation radius. For pressure diversion tunnel, take R_0=5.9m.

(4) Safety analysis on the area outside the blasting-induced fracture zone

The empirical formula proposed by Sadowski is used to describe the attenuation law of blasting vibration velocity in the zones far from the explosion sources, outside the blasting-induced fracture zone (Lu *et al.*, 2012). Its expression is:

$$V = \alpha (Q_{\max}^{1/3} / L)^{\beta} \tag{38}$$

Where, V represents peak vibration velocity, cm/s; and Q_{max} is the maximum explosive charge for single-section detonation, kg. For pressure diversion tunnel, Q_{max} =Q_b, and Q_b is the maximum explosive charge for single-section detonation of the breaking hole; α and β are the site influence coefficient and attenuation coefficient, respectively. L is the linear distance from the center of explosion, m.

According to the Formula (38), the blasting-vibration-influenced distance is:

$$L_{\text{sf}} = Q_{\max}^{1/3} (\alpha / V_{\text{sf}})^{1/\beta} \tag{39}$$

Where, L_{sf} is defined as the vibration-influenced distance of blasting, and outside the distance is the safe range under blasting vibration; V_{sf} is the safe velocity of vibration, and V_{sf}=7~12 cm/s is usually set for the hydraulic tunnel. For the Xi Luodu Hydropower Station, take V_{sf}=10 cm/s.

5. Numerical simulation and field test

5.1. Numerical simulation

(1) Geometric model

The FLAC3D finite difference numerical software is used for modeling. The specific geometric dimensions of the numerical model are shown in Figure 3, from where it can be seen that the overall shape of the model is cuboid. The cross section is 68.8 m high and 70.3 m wide. The model has an axial length of 80.0 m along the cavity. The excavated cavity is 47m long. The blasting loading zone is 3m long, and a semi-cylindrical hole is arranged on the excavation contour line as the equivalent blasting loading boundary of the perimeter hole.

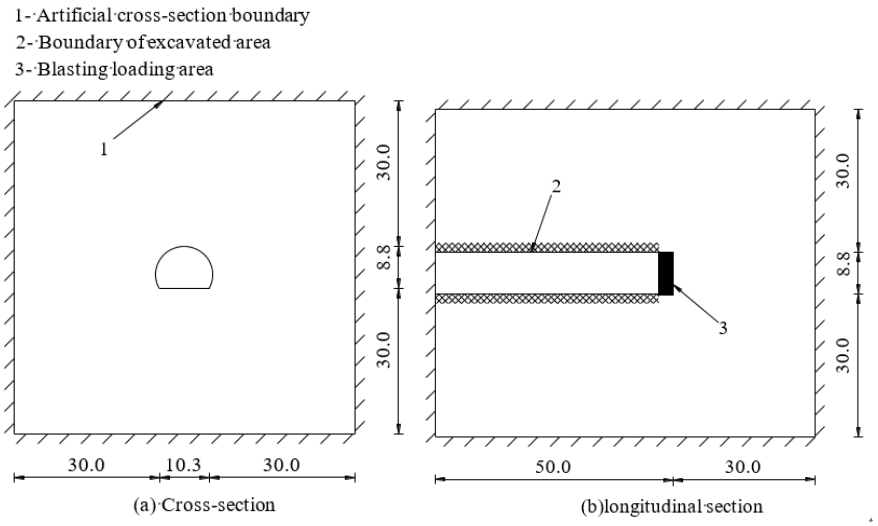

Figure 3. Section of numerical simulation model(unit: m)

(2) Boundary conditions

Static boundary conditions: The displacement constraint is imposed on the artificial boundary of the bottom of the model shown in Figure 3, and the corresponding original rock stresses is imposed on the other artificial boundaries as artificial boundary conditions for the static equilibrium state. The crustal stress parallel to the axial direction of the cavity is 6 MPa, the horizontal crustal stress perpendicular to the cavity axis is 16 MPa, and the vertical artificial stress at the top artificial boundary is 9 MPa. After the calculation of the static equilibrium of the cavity, the viscous non-reflective boundary is applied to the artificial boundary to absorb the reflected wave so as to reduce the influence of the artificial truncated boundary stress wave reflection on the calculation result.

Dynamic loading boundary conditions: As previously shown in Figure 2, the blasting loads of the breaking holes and the perimeter holes are applied to the corresponding equivalent loading boundaries in chronological order. The equivalent blasting load is calculated according to Formulas (6) and (7). Figures 4 and 5 show equivalent time history curves of the breaking hole and the perimeter hole, respectively, wherein the peak values of equivalent blasting loads of the breaking hole and the perimeter hole are 18.7 MPa and 400.MPa respectively, and the delay interval τ is taken as τ=1200 ms, according to actual project.

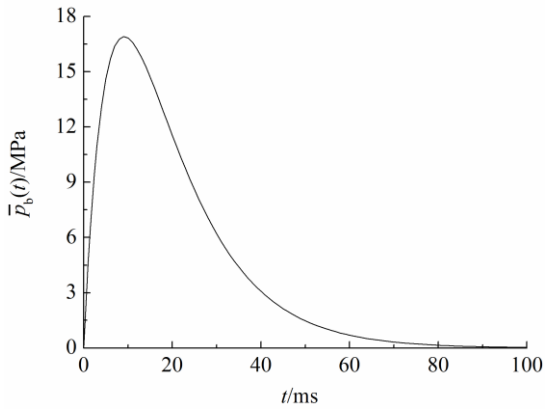

Figure 4. Curve of equivalent blasting load of breaking hole

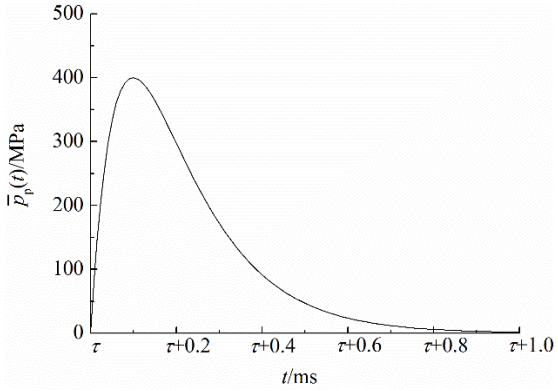

Figure 5. Curve of equivalent blasting load of perimeter hole

(3) Properties and constitutive relations of numerical material elements

The rock unit density is taken as 2,650 kg / m^3, the gravity acceleration as 9.8m / s^2, and values of bulk modulus and shear modulus of the intact rock as $\hat{K} = 40$ GPa and $\hat{G} = 24$ GPa. In view of the actual situation, the initial intactness index range is $0.2 \leq \eta \leq 0.8$, and the initial damage degree range is $0.2 \leq D_0 \leq 0.8$ according to the Formula (31). The constitutive relation of rock blasting damage determined by Formulas (28) and (29) is adopted, which is programmed into the numerical software FLAC3D.

In the numerical simulations, the parameters of drilling and blasting remain constant, but the initial intactness index η is changed, for the purpose of studying the influences of the intactness index.

5.2. Field test

The blasting test is carried out on site, and the main blasting parameters are shown in Table 1 above. The borehole acoustic wave test is carried out to check the failure of the surrounding rock near the explosion sources, using Rock Sea RS-ST01C ultrasonic wave tester. Before the blasting, the acoustic wave velocity is measured through the borehole acoustic wave test in zones not far from the blasting. The measured wave velocity is taken as the initial acoustic wave velocity and the initial damage degree is calculated using Formula (31). After blasting, drill holes on the profile after vertical excavation, inject water into the holes, and conduct acoustic wave test. The acoustic hole is about 6.0 m long, which is distributed in the vault, haunch and arch foot, etc. According to the damage criterion of blasting, D_{lim}, calculated by the Formula (32), the blasting-induced fracture depth of the surrounding rock is determined. The blasting vibration velocity is measured in the moderately far or far zones of the explosion, using TOPBOX. The blasting vibration velocity monitoring points are set up along the axial direction of the cavern near the intersection of the side wall and the bottom plate, and the monitoring direction is vertical and horizontal (pointing to the explosive center). The layout of the monitoring points is shown in Figure 6.

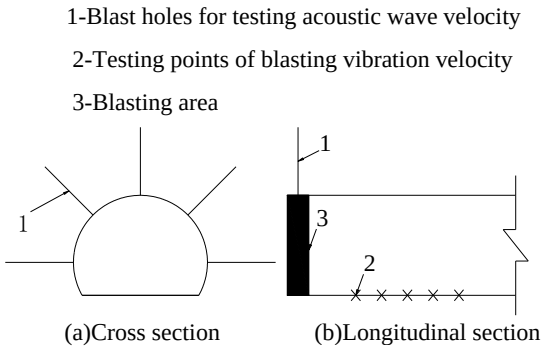

Figure 6. Monitoring points layout for the test

5.3. Analysis of test results

(1) Analysis of safety and stability in the zones near the explosion sources

Figure 7 is a nephogram of the distribution of blasting damage on the cross section with the initial intactness index η=0.6 and the initial damage degree D_0=0.4. In Figure 7, $1.0 \geq D \geq 0.4$, and different damage values D correspond to different degrees of damage. According to Formula (32), it can be obtained that D_{lim}=0.57. D_{lim} corresponds to the edge (point) of the affected range of blasting damage. The radial

distance between the edge line (point) and the contour line is the blasting-induced fracture depth. The comparison between the numerical calculation results and the field test results is shown in Figure 8, which reveals the distribution of the blasting-induced fracture zone on the cross section of the pressure diversion tunnel. It can be seen from Figure 8 that the blasting-induced fracture radius is gradually reduced from the haunch to the arch foot or the vault. The blasting-induced fracture depth ΔR is the smallest at the vault. Its numerical calculation and field test results are 0.16 m and 0.20 m, respectively, with a difference between the two of 0.04 m and the relative error of 20%. The blasting-induced fracture depth ΔR is the largest near the haunch of the arc about 1/4 from the vault, and $\Delta R=\Delta R_{lim}$. The numerical calculated value and the value obtained on site of $\Delta R_{lim}=0.6$ are 0.68 m and 0.60 m, respectively, with a difference of 0.08 m and a relative error of 13%.

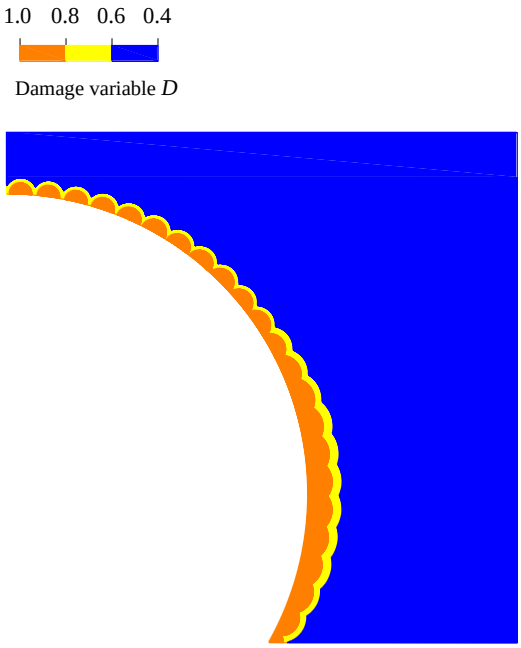

Figure 7. Blasting-induced damage nephogram of surrounding rock

Under the blasting load, the stress state at a certain point in the rock is the superposition result of the dynamic stress and the static stress of the original rock. For example, the circumferential total stress and the radial total stress near the perimeter hole are the superposition results of the circumferential dynamic stress and the radial dynamic stress with the original rock static stress, respectively. For the pressure diversion tunnel, the damage of the surrounding rock is mainly manifested by the radial expansion failure after the circumferential total tensile stress level exceeds the tensile strength of the rock. The circumferential static stress of the surrounding rock is determined by the redistribution of the vertical and horizontal stresses of the original

rock around the tunnel. The numerical calculation of the circumferential static stress of the surrounding rock is compressive stress. The maximum circumferential static stress of the vault on the cross-section is about 39 MPa, and it is parallel to the maximum horizontal crustal stress. The circumferential static stress at haunch is the minimum, about 12 MPa, and it is perpendicular to the maximum horizontal crustal stress. When the circumferential dynamic tensile stress caused by blasting is constant, the greater the circumferential static stress of the surrounding rock, the smaller the total circumferential tensile stress level, and the more difficult for the blasting damage to expand along the radial direction of the tunnel. Therefore, the blasting-induced fracture depth is the smallest near the vault and the largest near the haunch.

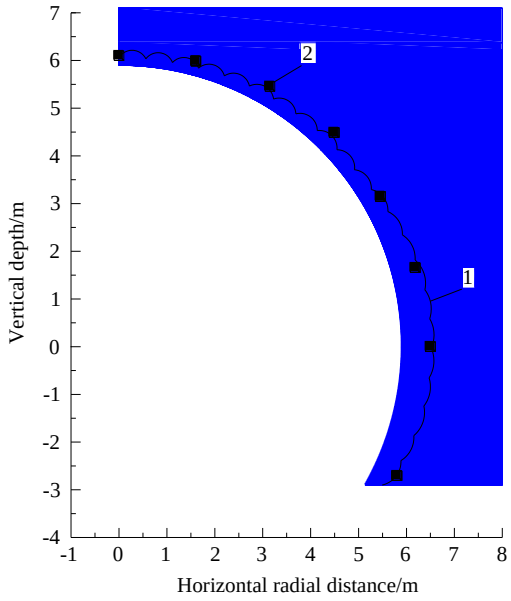

1- The blasting-induced fracture zone edge line obtained from numerical calculation, 2- The blasting-induced fracture zone edge points obtained from field test

Figure 8. Blasting-induced fracture zone of surrounding rock

When the charging parameters are constant, the relationship between the maximum blasting-induced fracture depth with the initial intactness index and the initial damage of the original rock according to Formulas (34)-(35) respectively are:

$$\Delta R_{\lim} = 6.23 \cdot (1 - D_0)^{-0.1} - 5.9 \tag{40}$$

$$\Delta R_{\lim} = 6.23 \cdot \eta^{-0.1} - 5.9 \tag{41}$$

The fitting correlation coefficients of the Formulas (40) to (41) are 0.98 and 0.98, respectively, with a respective range of $0.20 \leq D_0 \leq 0.80$ and $0.20 \leq \eta \leq 0.80$. The

maximum blasting-induced fracture depth along the radial direction of the retaining surrounding rock is well correlated with the intactness or the initial damage. The fitting curve of Formula (41) is shown in Figure 9, from where it can be seen that when the initial intactness index is reduced from 0.80 to 0.20, ΔR_{lim} increases from 0.43 to 1.28, with a nearly 2-fold increase, suggesting that the blasting damage range of surrounding rock increases obviously with the decrease of intactness index.

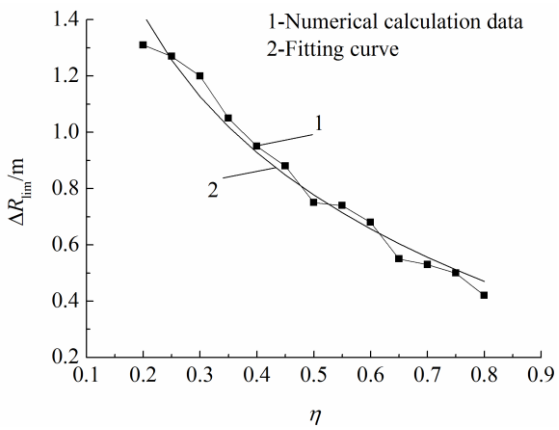

Figure 9. The relations between the maximum blasting-induced fracture depth and the initial intactness index of rock mass

(2) Analysis of safety and stability in the vibration zones which are not fractured by blasting

Table 2. Relations between blasting vibration velocity and propagation distance

Distance to the blasting center L/m	Peak vibration velocity in the horizontal direction V_H/(cm/s)		Peak vibration velocity in the vertical direction V_V/(cm/s)	
	Field test	Numerical calculation	Field test	Numerical calculation
10	18.3	20.3	19.7	21.5
15	12.6	10.2	13.2	10.9
25	5.6	5.4	4.8	4.7
35	4.1	3.4	2.8	2.7
50	1.8	1.7	1.7	1.6

Table 2 shows the relationship between the peak velocity of blasting vibration and the vibration propagation distance along the axial direction of the tunnel when the original rock intactness index is η=0.6. The special layout of the measuring points is shown in Figure 6 above. V_H and V_V are horizontal and vertical peak vibration velocities, respectively. It can be seen from Table 2 of the comparison of numerical calculation and field test results of the same measuring point, with the increasing distance from the blasting center, the absolute values of the relative error of horizontal vibration velocity successively are: 10.9%, 9.7%, 3.6%, 17.1%, and 5.5 %, and the absolute values of relative error of vertical vibration velocity successively are 9.1%, 17.4%, 1.5%, 3.5% and 5.9%. The numerical results are not different from the field test results, with the relative error of no more than 18%.

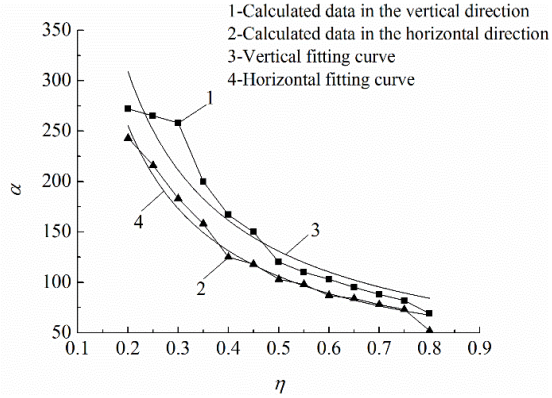

Figure 10. The relations between coefficient of site influence and intactness index of rock

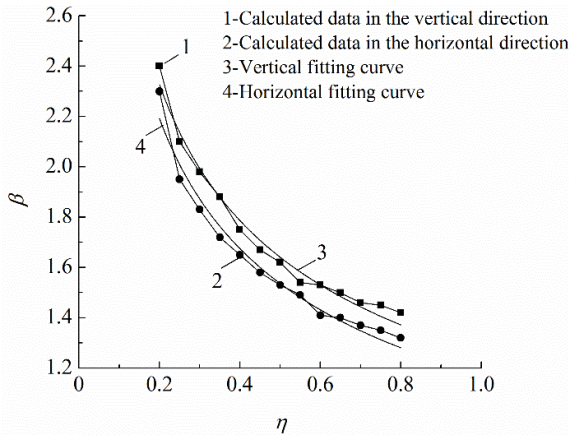

Figure 11. The relations between coefficient of attenuation and intactness index of rock

The relationship between the influence coefficient and attenuation coefficient of the blasting vibration site and the initial intactness index are shown in Figures 10 and 11, respectively, from where it can be seen that when the initial intactness index is $0.2 \leq \eta \leq 0.8$, the influence coefficient range of the blasting vibration site is $52 \leq \alpha \leq 272$, and the attenuation coefficient range is $1.32 \leq \beta \leq 2.40$. The influence coefficient and attenuation coefficient of the blasting vibration site in the vertical direction are greater than those in the horizontal direction. The influence coefficient and attenuation coefficient of blasting vibration site increase obviously with the decrease of initial intactness index. The fitting relationships of the curves in Figures 10 and 11 are calculated as follows:

$$\alpha_{\mathrm{V}} = 68.3 \cdot \eta^{-0.94} \tag{42}$$

$$\alpha_{\mathrm{H}} = 4.4 \cdot \eta^{-0.96} \tag{43}$$

$$\beta_{\mathrm{V}} = 1.26 \cdot \eta^{-0.38} \tag{44}$$

$$\beta_{\mathrm{H}} = 1.18 \cdot \eta^{-0.39} \tag{45}$$

In Formulas (42)-(45), α_{V} and α_{H} respectively are the influence coefficients of the blasting vibration site in the vertical and horizontal directions; and β_{V} and β_{H} the blasting vibration velocity attenuation coefficients in the vertical and horizontal directions; $0.2 \leq \eta \leq 0.8$, the fitting correlation coefficients are 0.95, 0.98, 0.97 and 0.98, respectively, with a good correlation.

For the pressure diversion tunnel, Figure 12 shows the relationship between the vibration-influenced distance of blasting and the intactness index of the original rock. As shown in Figure 12, in the numerical calculation results, when the intactness index is $0.2 \leq \eta \leq 0.35$, the blasting vibration-influenced distance L_{sf} increases from 14.0 m to 17.7 m with the increasing of the intactness index of the original rock η. When the intactness index of original rock is $0.35 \leq \eta \leq 0.80$, the blasting vibration-influenced distance L_{sf} fluctuates slightly with the increase of intactness index of the rock η, with an overall decreasing trend from 17.7 m to 12.2 m. The average value of blasting vibration-influenced distance is about 15.9 m. In the field test, the blasting vibration-influenced distance L_{sf} is the maximum, L_{sf} = 16.8m, when η=0.30, and subsequently, the vibration-influenced distance is gradually reduced. The laws obtained by numerical calculation and field test method are basically the same. When η=0.25, 0.30, 0.45, 0.60 and 0.75, the error absolute values of the numerical calculation relative to the field test are 8.0%, 4.0%, 3.0%, 7.2% and 10.8%, respectively, with the maximum relative error of no more than 11%. The distance between concrete pouring position and explosion source shall be greater than the vibration-influenced distance. Therefore, inside the vibration-influenced distance, bolting and shotcreting for surrounding rock shall be carried out in time according to its conditions. The vibration-influenced distance of blasting in the constructions of Xi Luodu Hydropower Station is generally

10-15 m, which does not report much difference from the calculated result 12.2-17.7 m.

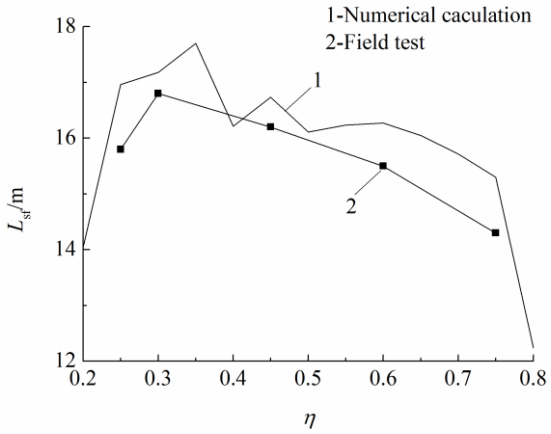

Figure 12. The relation between the vibration-influenced distance and intactness index of rock

6. Conclusions

Against the actual blasting excavation project of pressure diversion tunnels, this study uses numerical simulations and field tests to jointly discuss the influences of the initial intactness index of rock mass on the safety and stability of the tunnels. In this study, the method of using the equivalent blasting load to replace the actual multi-holes blasting load is presented to simplify the numerical simulation of multi-holes blasting and the blasting damage model considering the influences of the intactness index of rock mass on blasting effects is established. According to this study, there are the main conclusions as follows:

(1) The initial intactness of rock mass has significant influences on the blasting dynamic responses of the surrounding rock of tunnels, including the blasting-induced fracture near the explosion sources and the blasting vibration far from the explosion sources, outside the blasting-induced fracture zones. For the blasting excavation project of pressure diversion tunnels, under the conditions that the parameters of drilling and blasting remain constant, the maximum blasting-induced fracture depth, as well as the site influence coefficient and the attenuation coefficient based on the Sadowski's formula for predicting the peak particle velocity induced by blasting vibration, decreases with the increasing of the initial intactness index.

(2) In the established blasting damage model, the relation between the intactness index of rock mass before blasting and the damage variable was given, so that the changes of the intactness index can be used to consider the influences of rock mass intactness on blasting effects. As the initial intactness index of rock mass is easy to obtain by measuring the acoustic wave velocity, the established model can be

conveniently applied in analysis of the influences from the intactness of rock mass on the safety and stability of actual projects during blasting excavations.

(3) Due to the complicated factors in field and the simplification of the theoretical model, there are some differences between the numerical results and the field test results. However, the maximum error between the two is generally less than 20%, thus the numerical results can basically meet the engineering requirements, and the blasting damage model and the method of equivalent blasting loading are reasonable. The research results of this study have certain limitations, but they can provide references for similar projects in safety assessment of blasting excavation.

Reference

Bhandari S., Badal R. (1990). Post-blast studies of jointed rocks. *Engineering Fracture Mechanics*, Vol. 35, No. 1, pp. 439-445. https://doi.org/10.1016/0013-7944(90)90221-2

Cai D., Zhang J. (1997). Numerical simulation and application of blasting damage of bed rock mass. *Journal of Hydraulic Engineering*.

Chen E. P., Taylor L. M. (1986). Fracture of brittle rock under dynamic loading condition. *Fracture Mechanics of Ceramics*, No.7, pp. 175-186. https://doi.org/10.1007/978-1-4615-7023-3_13

Chen J. H., Li X. P., Zhang J. S. (2016). Study on blasting parameters of protective layer excavation of rock bench based on blasting-induced damage. *Chinese Journal of Geotechnical Engineering*, Vol. 35, No. 1, pp. 98-108. https://doi.org/10.13722/j.cnki.jrme.2014.1501

Chen J. H., Zhang J. S., Li X. P. (2016). Model of rock blasting-induced damage and its application based on the integrity of rockmass. *Chinese Journal of Geotechnical Engineering*, Vol. 38, No. 5, pp. 857-866. https://doi.org/10.11779/CJGE201605011

Chen J. H., Zhang J. S., Li X. P. (2016). Study of presplitting blasting parameters and its application based on rock blasting-induced damage theory. *Rock and Soil Mechanics*, Vol. 37, No. 5, pp. 1441-1450. https://doi.org/10.16285/j.rsm.2016.05.028

Chen M., Lu W. B., Yan P., *et al.* (2015). Blasting excavation induced damage of surrounding rock masses in deep-buried tunnels. *KSCE Journal of Civil Engineering*, Vol. 20, No. 2, pp. 933-942. https://doi.org/10.1007/s12205-015-0480-3

Furlong J. R., Davis J. F., Alme M. L. (1990). modeling the dynamic load/unload behavior of ceramics under impact loading. RDA-TR-0030-0001, Arlington, VA: R& D Associates, Arlington,1990.

Grady D. E., Kipp M. E. (1980). Continuum modelling of explosive fracture in oil shale. *International Journal of Rock Mechanics and Mining Sciences*, No. 17, pp. 147-157. https://doi.org/10.1016/0148-9062(80)91361-3

Kipp M. E., Grady D. E. (1980). Numerical studies of rock fragmentation. *Computers & Chemical Engineering*, pp. 721-735.

Kuszmaul J. S. (1987). A new constitution model for fragmentation of rock under dynamic loading. *Proceedings of the 2nd International Symposium on Rock Fragmentation by Blasting*, pp. 412-423.

Li N. (1994). A numerical model for blast load and its application. *Chinese Journal of Rock Mechanics and Engineering*, Vol. 13, No. 4, pp. 357-364.

Li X. P., Chen J. H., Li Y. H., *et al.* (2010). Study of criterion and damage zone induced by excavation blasting of underground power-house of Xiluodu hydropower station. *Chinese Journal of Rock Mechanics and Engineering*, Vol. 29, No. 10, pp. 2042-2048.

Liu L. Q., Katsabanis P. D. (1997). Development of a continuum damage model for blasting analysis. *International Journal of Rock Mechanics and Mining Sciences*, Vol. 34, No. 2, pp. 217-231. https://doi.org/10.1016/S0148-9062(96)00041-1

Lu W. B., Hustrulid W. (2002). An improvement to the equation for the attention of peak particle velocity. *Engineering Blasting*, Vol. 8, No. 3, pp. 1-4.

Lu W. B., Luo Y., Chen M., *et al.* (2012). An introduction to Chinese safety regulations for blasting vibration. *Environmental Earth Sciences*, Vol. 67, No. 7, pp. 1951-1959. https://doi.org/10.1007/s12665-012-1636-9

Ma G., An X. M. (2008). Numerical simulation of blasting-induced rock fractures. *International Journal of Rock Mechanics & Mining Sciences*, Vol. 45, No. 6, pp. 966-975.

Ramulu M., Sitharam T., Chakraborty A. (2009). Rock mass damage assessment due to repeated blast vibrations due to open cut blasting on underground granite rock mass at a hydroelectric construction projects. *Journal of the American Statistical Association*, Vol. 97, No. 459, pp. 924-925. https://doi.org/10.2307/3085740

Saiang D. (2010). Stability analysis of the blast-induced damage zone by continuum and coupled continuum–discontinuum methods. *Engineering Geology*, Vol. 116, No. 1, pp. 1-11. https://doi.org/10.1016/j.enggeo.2009.07.011

Saiang D. (2010). Stability analysis of the blast-induced damage zone by continuum and coupled continuum–discontinuum methods. *Engineering Geology*, Vol. 116, No. 1, pp. 1-11. https://doi.org/10.1016/j.enggeo.2009.07.011

Taylor L. M., Chen E. P., Kuszmaul J. S. (1986). Microcrack-induced damage accumulation in brittle rock under dynamic loading. *Computer Methods in Applied Mechanics and Enginering*, Vol. 55, No. 3, pp. 301-320. https://doi.org/10.1016/0045-7825(86)90057-5

Taylor L. M., Kuszmaul J. S., Ghen E. P. (1985). Damage accumulation due to macrocracking in brittle rock under dynamic loading. *American Society of Mechanical Engineers*, No. 69, pp. 95-104.

Wang Z. L., Konietzky H. (2009). Modelling of blast-induced fractures in jointed rock masses. *Engineering Fracture Mechanics*, Vol. 76, No. 12, pp. 1945-1955. https://doi.org/10.1016/j.engfracmech.2009.05.004

Yang R., Brwden W. F, Katsabanis P. D. (1996). A new constitutive model for blast damage. *International Journal of Rock Mechanics and Mining Sciences*, Vol. 33, No. 3, pp. 245-254. 10.1016/0148-9062(95)00064-X

Zhao H. B., Long Y., Li X. H., *et al.* (2016). Experimental and numerical investigation of the effect of blast-induced vibration from adjacent tunnel on existing tunnel. *KSCE Journal of Civil Engineering*, Vol. 20, No. 1, pp. 431-439. https://doi.org/10.1007/s12205-015-0130-9

Zhu C. Y., Yu S. C. (2001). Study on the criterion of rockmass damage caused by blasting. *Engineering Blasting*, Vol. 7, No. 1, pp. 12-16.

Zuo S. Y., Xiao M., Xu J. K., *et al.* (2011). Numerical simulation of dynamic damage effect of surrounding rocks for tunnels by blasting excavation. *Rock and Soil Mechanics*, Vol. 32, No. 10, pp. 3171-3176. https://doi.org/10.1177/0883073810379913